SLAC-PUB-16489

Enhanced ion acceleration in transition from opaque to transparent plasmas

R. Mishra, F. Fiuza and S. Glenzer

SLAC National Accelerator Laboratory
2575 Sand Hill Road, Menlo Park, CA 94025, U.S.A

E-mail: rmishra@slac.stanford.edu and fiuza@slac.stanford.edu

Abstract.

Using particle-in-cell (PIC) simulations, we investigate ion acceleration in the interaction of high intensity lasers with plasmas which transition from opaque to transparent during the interaction process. We show that the highest ion energies are achieved when the laser traverses the target around the peak intensity and re-heats the electron population responsible for the plasma expansion, enhancing the corresponding sheath electric field. This process can lead to an increase of upto 2x in ion energy when compared with the standard Target Normal Sheath Acceleration (TNSA) in opaque targets under the same laser conditions. A theoretical model is developed to predict the optimal target areal density as a function of laser intensity and pulse duration. A systematic parametric scan for a wide range of target density and thickness is performed in 1D and 2D and shown consistent with the theory. These results open the way for a better optimization of the ion energy in future laser-solid experiments.

PACS numbers: 41.75.Jv, 52.38.Kd, 52.50.Jm

This material is based upon work supported by the U.S. Department of Energy, Office of Science, Office of Basic Energy Sciences, under Contract No. DE-AC02-76SF00515.

1. Introduction

Advances in the development of intense short pulse lasers have led to exciting progress in plasma-based ion acceleration. Production of energetic ion bunches from compact laser-plasma systems have attracted great attention due to the wide range of potential applications, from injectors for conventional accelerators, to proton imaging and oncology [1, 2, 3, 4, 5, 6].

Several laser-driven ion acceleration regimes have been explored over the last decade. For a given laser pulse, the target conditions determine the dominant acceleration mechanism(s). In solid density targets the most studied ion acceleration mechanisms, both theoretically and experimentally, are Target Normal Sheath Acceleration (TNSA) [7] and Radiation Pressure Acceleration (RPA)[8]. However, despite continuous increase in laser energy and power, the maximum ion energy produced has been limited to 70 MeV [9], which together with poor spectral quality is still insufficient for many applications of interest. More recently ion acceleration has also been explored in near critical density plasmas via laser Shock Wave Acceleration [10, 11, 12, 13] and Magnetic Vortex Acceleration [14, 15, 16], being compatible with high repetition rate systems and promising a better control over the ion beam properties. An interesting intermediate regime is that of the laser induced relativistic transparency [17, 18] where the target is initially opaque but due to electron heating and expansion it becomes transparent during the laser interaction. Promising experimental results have been reported that show an enhancement of the ion energy [19, 20]. However, the physical picture responsible for this enhancement and the optimal conditions for ion acceleration are not yet clear.

In this paper, we study laser ion acceleration in relativistic transparency regime where the target is initially opaque to the incident laser but becomes transparent due to fast plasma expansion driven by laser produced hot electrons. We show that for a given laser there is an optimal electron arial density that will produce the highest ion energy in this regime. We carried out 1D and 2D simulations using the fully-relativistic, fully-electromagnetic particle-in-cell (PIC) code PICLS [21, 22] to investigate the details of the process. We observed in the simulations that the peak ion energy is enhanced if the laser crosses the target and re-heats the electrons in the expanding sheath region. In order to optimize this enhancement process we derive a simple theoretical model to predict optimal conditions for ion acceleration in the framework of laser transparency. The theoretical model predicts an optimal electron areal density dependence on laser parameters, $\frac{n_{e0}}{n_c} L_0[\mu m] \propto \tau_p I_0^{3/4}$ to produce the highest ion energies. Here, n_{e0}, n_c, L_0, τ_p, and I_0 are initial plasma electron density, non-relativistic electron critical density, initial target thickness, laser full-width-half-maximum (FWHM) pulse duration, and laser peak intensity, respectively. We benchmark the analytical model with PIC simulations and find good overall agreement. In particular, the analytical model correctly describes the dependence of optimal arial density on laser parameters such as peak intensity and pulse duration. For example, for presently available high intensity laser systems ($a_0 \sim 10 - 15$, $\tau_p \sim$ 100fs) the highest ion energy can be produced either with 50 nm thick, 200 n_c targets or with μm thick, $10 n_c$ targets, which are yet to be used experimentally. The results from this study will allow for a better design and interpretation of laser-solid experiments focusing on ion acceleration with thin solid density targets.

This paper is organized as follows. In section 2, we present detailed results from a 2D simulation for short pulse laser-solid interaction in the transparency regime.

We show that when the laser crosses the target, the peak ion energy is boosted compared to conventional TNSA where the target remains opaque throughout the interaction process. In section 3, we present a simple analytical model to predict optimal conditions for ion acceleration based on the 1D-like expansion of the target. We then compare the analytical model with a 1D and 2D PIC parameter scan in section 4 and show good overall agreement. Finally, in section 5, we present the main conclusions.

2. Ion acceleration in transition to transparent regime

TNSA typically occurs when a laser interacts with a solid density foil. The laser-plasma interaction produces hot electrons with temperature T_{hot} which escape the target setting up a strong ($\sim$ TV/m) space-charge sheath electric field on the target surface which scales as $E \propto T_{hot}/\lambda_D$ where λ_D is the characteristic hot electron Debye length [23, 24, 25]. This sheath electric field accelerates ions which are confined in the expanding sheath electron cloud. The large space charge field in theory can accelerate ions to very high energies, however due to the large ion inertia electrons are pulled back and cool in the process reducing the sheath electric field. A substantial improvement in the ion energy gain would be achieved if the electron energy in the expanding sheath region is continuously replenished rather than the electron-ion interaction progressing as an adiabatic process. This possibility may occur if the target becomes transparent allowing the laser to cross and re-heat the electrons that are driving the expansion in the acceleration region.

We have performed PIC simulations in a 2D geometry in order to confirm this possibility and identify the main aspects of the interplay between TNSA and relativistic transparency in determining the optimal conditions for ion acceleration. The laser is p-polarized and has a gaussian temporal profile with a peak intensity $I_0 \approx 2 \times 10^{20}$ W/cm^2 ($a_0 \approx 12$), here a_0 is the (dimensionless) normalized laser amplitude $a_0 = 8.55 \times 10^{-10}\lambda_0[\mu\text{m}]\sqrt{I_0[\text{Wcm}^{-2}]}$. The laser wavelength is set at λ_0= 1 μm and focal spot size is 5 μm. The total laser pulse duration is $942\omega_0^{-1} \approx 500$fs, with the FWHM of $521\omega_0^{-1} \approx 273$fs, here $\omega_0 = 2\pi c/\lambda_0$ is the laser angular frequency. The simulation domain is $80\mu m$ in the laser propagation (x) direction and $50\mu m$ in the transverse (y) direction. The spatial and temporal resolution used in the simulations are $\lambda_0/125$ and $2\pi\omega_0^{-1}/125$, respectively. The total number of particles per cell is 100. We have also used absorbing boundaries for particles and electromagnetic waves. For the laser described above we have tested different target thickness conditions for proton acceleration. We illustrate the optimal case, here defined as run A, where the peak proton energy was maximized. In run A, we used a $2.5\mu m$ thick hydrogen target with sharp boundaries and with density of $15n_c$. The target is initially cold in the simulation and the front surface of the target is at $20\mu m$ from the left boundary.

Figure 1 shows the temporal evolution of the laser plasma interaction from the 2D PICLS simulation. When the laser starts to interact with the target surface, since the target is initially opaque to the laser, its penetration is limited to the skin depth layer ($l_s = c/\omega_{pe}$), here ω_{pe} is the electron plasma frequency given as $\omega_{pe}^2 = 4\pi e^2 n_{e0}/m_e$. Earlier in the laser interaction (t $\approx$ 100fs), while the laser is in its rising edge, we see that the laser has slightly compressed the target front surface (Fig. 1(a)) and is partially absorbed in the interaction region producing hot electrons mostly via $\vec{J}\times\vec{B}$ heating [26, 27]. In Fig. 1(j) we see the characteristic 2ω electron bunches from $\vec{J}\times\vec{B}$ heating spaced at $\lambda_0/2$. This leads to a typical sheath electric field being produced on

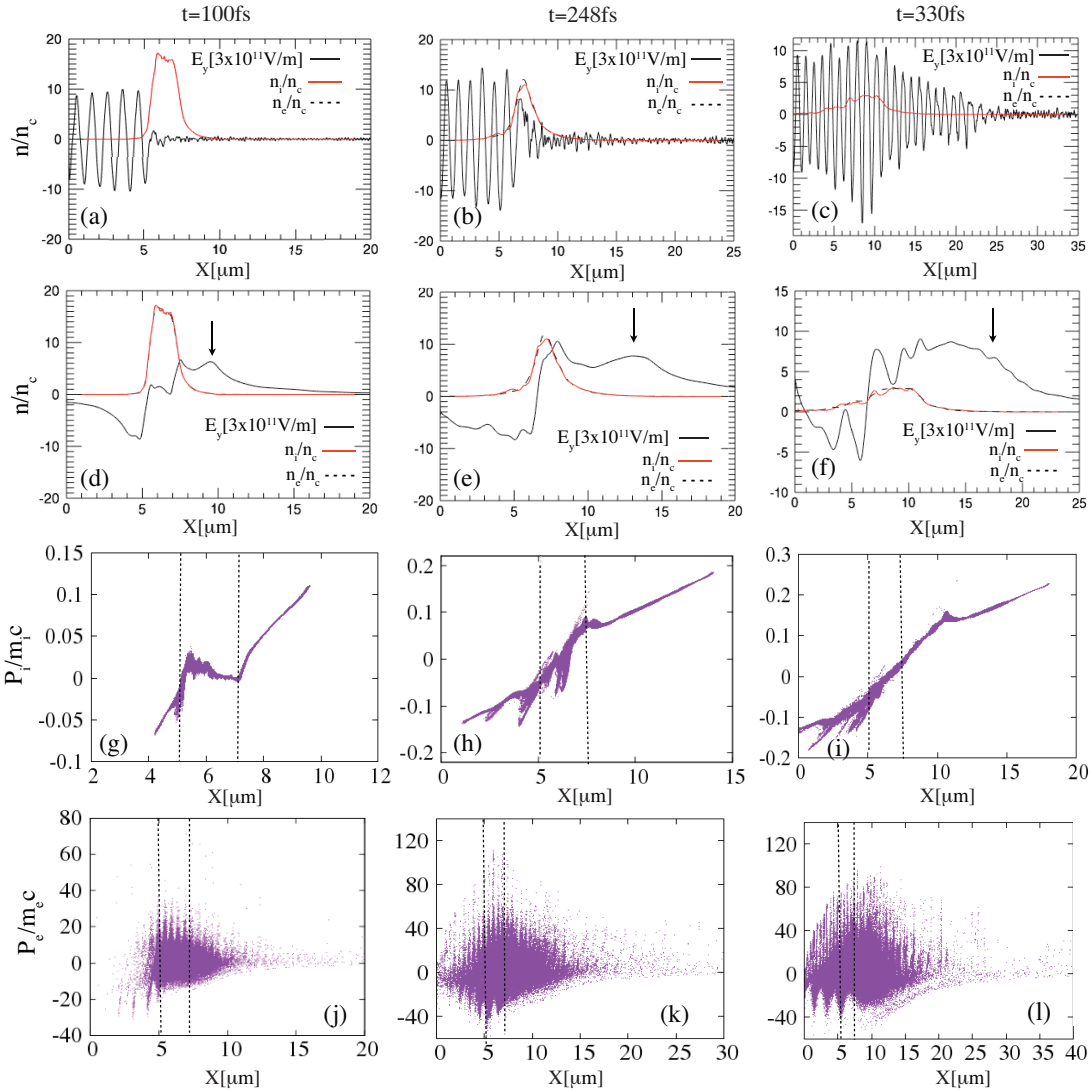

Figure 1. Temporal evolution of laser plasma interaction for proton acceleration in laser transparent regime. Rows 1 to 4 show the laser electric field (E_y), longitudinal plasma electric field (E_x), electron, and ion phase space, respectively. The two top rows also show the ion (n_i) and electron (n_e) densities. Columns 1 to 3 correspond to interaction times of t=100fs, 248fs, and 330fs. Black arrows correspond to the front of the accelerated ions. Black dotted vertical lines on the phase-space plots show the target initial boundaries (X=5μm to 7.5μm).

the vacuum target boundaries (Fig. 1(d)), and to the acceleration of protons by TNSA (Fig. 1(g)). As the hot electrons drive the plasma expansion the peak electron density starts to drop and at t $\approx$ 248fs (Fig. 1(b,e)) reaches the relativistic transparency condition [28, 29], *i.e.* the relativistically correct critical density $n_e \sim \gamma_0 n_c$, where

$\gamma_0 = (1 - v_0^2/c^2)^{-1/2}$ is the Lorentz factor of the electrons quivering in the laser field. At this point the plasma transitions from opaque to transparent. This allows the laser to penetrate through the bulk of the target (Fig. 1 (b,c)) and re-heat the hot electrons in the expanding sheath region (Fig. 1 (k,l)) resulting in an increase in the peak sheath electric field E_x on the rear side, as seen in Fig.1(e) and Fig.1(f).

It is also important to note that the group velocity of the laser as it crosses the near critical density plasma, $v_g = c\sqrt{1 - n_e/(\gamma_0 n_c)}$, can be significantly lower than c, thus allowing the laser to interact for an extended period of time with the expanding structure. This leads to a re-heating of the electrons and allows the enhanced TNSA electric field E_x to decay slowly as it directly depends on the hot electron temperature. Proton acceleration in such enhanced TNSA field results in higher peak proton energies compared to the conventional TNSA process where the laser stops at the front surface.

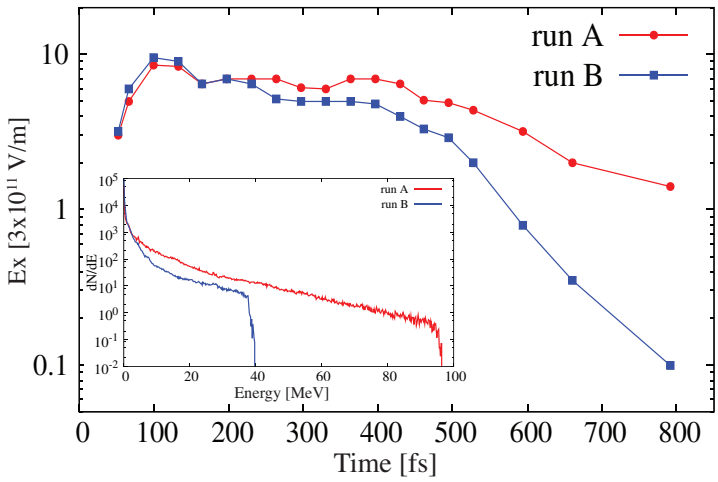

Figure 2. Local peak TNSA electric field present at expanding ion front in run A (red curve) and run B (blue curve). In run A sheath field decays slower due to re-heating of expanding electrons as the laser crosses the plasma. Proton spectra from run A (red curve) and run B (blue curve) are shown in the inset. Protons gain more than twice the energy in run A due to enhanced TNSA.

In order to quantify the enhancement of the standard TNSA electric field due to laser penetration and interaction with the expanding plasma, we have performed a similar 2D simulation, hereafter referred to as run B. In this case we use a slightly higher target density of $23n_c$ to insure that the target remains opaque to the laser light during the laser interaction. The target thickness in run B is $2\mu m$, such that the areal mass density is only 12% higher than in run A. It is reasonable to assume that the laser absorption should not be significantly different due to such small difference in target parameters. In Fig. 2, we show the evolution of transversely averaged (over laser focal spot) peak sheath electric field present at the accelerating ion front for run A and run B. Note that in run A the laser starts to penetrate the bulk plasma around 250 fs. As seen in Fig. 2, before the onset of relativistic transparency in run A ($t \approx 250$ fs) the peak TNSA sheath fields are comparable. This confirms that the laser absorption and TNSA are indeed similar, which allows us to make a quantitative comparison in the evolution of the sheath fields in expanding rear sides in both simulations. After

the onset of laser transparency in run A the differences become significantly larger. Note that after the laser pulse ends in run B the peak electric field falls very rapidly. However, in run A not only the sheath field is enhanced but it also decays slower. This plays an important role in the efficiency of ion acceleration in the transparency regime. A typical TNSA-like proton spectrum is observed in both runs but with the peak proton energy twice as high in run A compared to run B, as shown in the inset of Fig. 2. In the case of opaque target (run B), the maximum proton energy is ≈ 40 MeV, consistent with previous experimental results. In the case where the target becomes transparent (run A) the maximum energy reaches ≈ 95 MeV. This shows that if the laser-target parameters are optimized it is possible to significantly increase the peak ion energy in this regime.

In the simulations, we have observed that the optimal conditions for acceleration (i.e. maximization of ion energy) are achieved if the target becomes transparent when the laser is interacting around its peak intensity. On the one hand, by this time the highest hot electron temperature is achieved, leading to the strongest TNSA acceleration at the rear side of the target. On the other hand, it allows for the transmission of a significant fraction of the laser energy ($\approx 50\%$) through the target, which will further heat the electrons, maintaining a strong TNSA field for longer time. If transparency occurs too early in the laser pulse, the TNSA field is weak and the laser crosses without interacting for significant time and heating the expanding electrons. If transparency occurs too late in the laser pulse, only a small fraction of the laser energy will reach the rear side, not allowing for a strong re-heating of the electrons. In the next section, based on this observation, we construct a simple analytical model for the optimal conditions for acceleration in this laser transparency regime.

3. Analytical Model

We start by considering a thin one dimensional step-like density profile for the plasma target with the initial density n_{e0} and thickness L_0. The electrons and ions in the target are initially cold and at rest. Electrons are then heated by a p-polarized gaussian laser pulse incident on the plasma target. The laser pulse is characterized by the wavelength λ_0, the FWHM duration τ_p and the laser (dimensionless) normalized amplitude a_0. We consider that the target is initially opaque to the laser light *i.e.* $n_{e0} > \gamma_0 n_c$ and also $\lambda_D \ll L_0$. For a p-polarized laser γ_0 can also be defined as $\gamma_0 = \sqrt{1 + a_0^2/2} \approx a_0/\sqrt{2}$ for $a_0 \gg 1$. As the laser interacts with the target, electrons are strongly heated and lead to target expansion. For simplicity, we assume a 1D-like expansion where the areal mass density of the target will be conserved

$$n_{e0} L_0 = n_e L. \tag{1}$$

During the expansion, the thickness of the target evolves as $L \simeq L_0 + 2\, c_s\, t$, where $c_s = \sqrt{Z k_B T_{hot}/m_i}$ is the ion sound speed, Z, k_B, T_{hot} and m_i are the atomic number, Boltzmann constant, fast electron temperature and ion mass, respectively. The fast electron temperature is defined by laser ponderomotive scaling $k_B T_{hot} = \left(\sqrt{1 + \frac{a_0^2}{2}} - 1\right) m_e c^2 \approx \frac{a_0}{\sqrt{2}}\, m_e c^2$.

In order to maximize ion acceleration the target should become relativistically transparent, *i.e.* $n_e \approx a_0/\sqrt{2} n_c$, near the peak of laser intensity ($t \approx \tau_p/2$) as observed in the simulations discussed in Fig. 1. In the limit of high laser intensity ($a_0 \gg 1$) (which is the limit of interest for the generation of high energy ion beams), by the

time the laser reaches peak intensity the expansion of the target largely exceeds the initial target thickness L_0. Under this assumption and after substituting n_e and L on right side of Eq. (1), we arrive at an expression for the optimal areal density of the target as a function of the laser parameters

$$\frac{n_{e0}}{n_c} L_0 \approx c\,\tau_p \sqrt{\frac{a_0^3}{2^{3/2}} \frac{Z\,m_e}{m_i}} \approx 0.59\,c\,\tau_p \sqrt{a_0^3 \frac{Z\,m_e}{m_i}}. \tag{2}$$

Eq. (2) predicts that there is an optimal electron areal density for a given set of laser conditions (peak intensity and pulse duration) to produce the highest ion energies in the interaction of intense lasers with solid density targets in the laser transparency regime.

4. Comparison with PIC simulations

In order to test the validity of our model we have performed a wide parameter scan using the 1D and 2D PICLS simulations. We have changed the laser and target parameters systematically to understand which combination of parameters leads to the highest ion energies and to compare that with the theoretical prediction from Eq. (2).

We consider a Hydrogen plasma with solid density $40n_c$ and change the target thickness for (i) different laser amplitude a_0, ranging from 5 to 20, while keeping the FWHM pulse duration $\tau_p \approx 112$fs, (ii) different FWHM pulse duration τ_p, ranging from 50fs to 500fs, while keeping the laser $a_0 \approx 10$. The choice of Hydrogen for the plasma target is motivated by the recent development of cryogenic Hydrogen jets at the Matter Under Extreme Condition (MEC) end station at SLAC which can be used for ion acceleration experiments. For Hydrogen, solid density is $\approx 40n_c$ for a 1μm wavelength laser. Hydrogen cryogenic jets with tunable thickness (1μm - $20\mu m$) provide the opportunity to explore proton acceleration from a pure hydrogen source of solid density. The results from this set of simulations are shown in Fig. 3(a) and Fig. 3(b) for a_0 and τ_p dependence, respectively. We find that for a given laser a_0 and τ_p there is indeed an optimal electron areal density for which the protons have achieved the highest energy during the interaction. The optimal areal density from 1D and 2D simulations follows the same trend as predicted in Eq. (2). The results from 2D simulations are in better quantitative agreement with theory. This is mostly associated with the fact that in 1D simulations with a sharp density profile it takes a significant time for the laser absorption and electron heating to increase [27] and the hot electron temperature is underestimated. In 2D, we have confirmed that the hot electron temperature is close to the ponderomotive scaling used in the analytical model. We clearly observe that the optimal density increases for either increasing laser a_0 or pulse duration τ_p, *i.e.* it increases with increasing laser energy. Detailed analysis of the simulations confirms that for targets much thinner than the optimal condition the laser penetrates the plasma too early before a significant TNSA field is established. As the laser crosses the target it interacts with the expanding plasma only in a short region and does not provide a significant increase in the proton acceleration. Similarly, for much thicker targets, the laser penetrates the target only later in the falling edge, when most of the laser energy has been reflected/absorbed and the re-heating of sheath electrons is not efficient. We have also verified in the simulations that for the optimal areal density the laser crosses the target shortly after

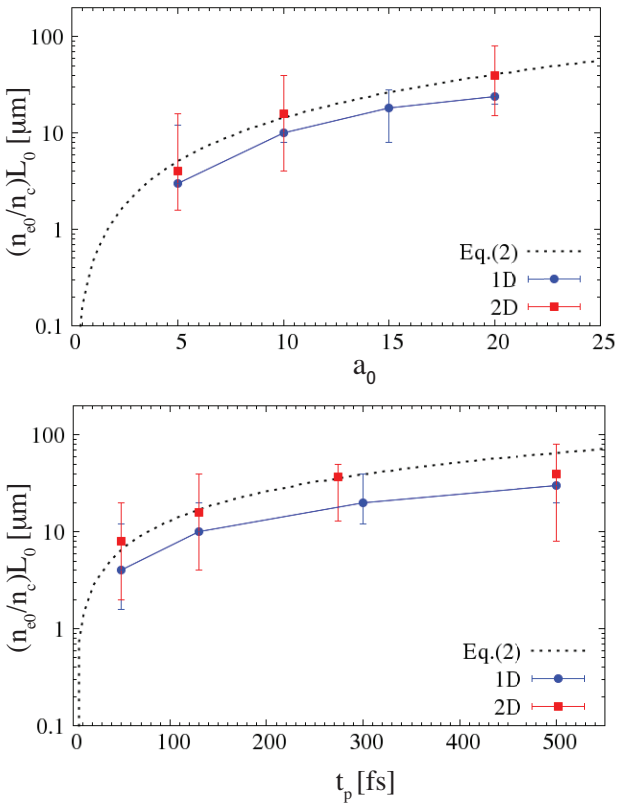

Figure 3. Normalized optimal electron areal density $(n_{e0}/n_c)L_0[\mu m]$ as predicted in Eq. (2) for Hydrogen (solid line) and in 1D (blue curve) and 2D (red solid circles) PICLS results for highest proton energy as a function of laser a_0 (top) and laser FWHM pulse duration (bottom).

its peak intensity which appears to be the most important condition. Our results show that in micron-scale Hydrogen jets optimal proton acceleration is achieved for $a_0 \approx 20$. Note that the optimal areal density prediction from Eq. (2) is also consistent with previous experimental results [19, 20] that showed evidence of an optimal target thickness and density at which the ion energy is maximized. We also note that our results are different from previous analytical and numerical work on the optimization of the proton energy for thin targets, where no dependence on laser duration has been derived and the analysis was mostly focused on the Coulomb explosion regime [30].

We have also done a large 1D parameter scan, where we varied both target density and the thickness. Table 1 shows the peak proton energy observed for different areal densities as function of the target thickness (variation along the column) or density (variation along the row). The target densities were varied from $6n_c$ to 600 n_c, whereas target thickness ranges between 10nm to 10μm. The laser peak intensity is fixed at 1.5×10^{20} W/cm^2, which corresponds to $a_0 \approx 10$. FWHM pulse duration and wavelength are 273 fs and 1μm, respectively. The peak proton energy obtained in the simulations for each set of varying thicknesses and densities is shown in Table 1, with the higher proton energies highlighted in bold. We clearly observe that there is

	Peak proton energy [MeV]			
L_0 [μm]	$n_{e0} = 10n_c$	$n_{e0} = 40n_c$	$n_{e0} = 100n_c$	$n_{e0} = 600n_c$
0.01	1.4	20	108	220
0.04	3	70	250	**350**
0.1	10	215	**376**	130
0.5	175	**360**	100	70
2.0	**350**	125	52	50
5.0	130	50	55	40

Table 1. 1D PICLS parameter scan on target thickness and density for proton acceleration in hydrogen plasma. Laser $a_0 = 10$ and FWHM pulse duration is 273 fs. Maximum proton energy is in bold and corresponds to the optimal areal density.

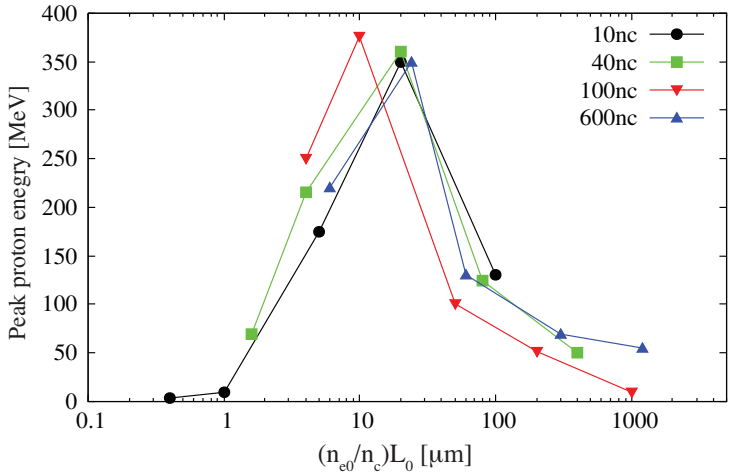

Figure 4. Maximum proton energy over a large range of target density and thickness. The laser intensity is 1.5×10^{20}W/cm^2 ($a_0 = 10$) and duration is 273 fs. Optimal acceleration is observed for $(n_{e0}/n_c)L_0[\mu m] \approx$ 10 - 24.

an optimal condition for acceleration that corresponds to fixed areal density, $n_{e0}L_0$, which falls along the diagonal of the table.

This is also illustrated in Fig. 4, where we plot the peak proton energy as a function of areal density for the different cases. Indeed the maximum proton energy is reached for an optimal areal density of $n_{e0}/n_cL_0[\mu m] \approx$10 - 24. The difference to our analytical prediction ($n_{e0}/n_cL_0[\mu m] \approx 36$) is in large part associated with the weak laser absorption in 1D, as explained above. It is remarkable that this optimal areal density is maintained for such a wide range of thicknesses associated with current laser-solid experiments and that the peak proton energy is approximately the same independent of the actual target thickness or density.

We note that the focus of this comparison, in particular using 1D simulations, is on understanding the validity of the analytical model in predicting the optimal target conditions that lead to the highest ion energies for a given laser, and not on the prediction of the exact ion energies as 1D simulations clearly overestimate the ion energy.

5. Discussion

In conclusion, we have shown that optimal ion acceleration can be achieved when the target becomes relativistically transparent at the peak intensity of the laser pulse interaction. This allows the remaining fraction of the laser to cross the target and re-heat the electrons, enhancing the sheath field at the rear side of the target. We have derived a simple analytical model that shows that for a given set of laser conditions there is an optimal target areal density to produce the highest energy ions in the laser transparent regime. This optimal areal density scales as $\tau_p I_0^{3/4}$, which is in very good agreement with 1D and 2D PIC simulations. We also show that for a given laser this optimal areal density remains fairly constant over a wide range of target densities and thicknesses. To date, most of the experimental work exploring ion acceleration in the relativistic transparency regime used high density nanometer thick targets [19]. Our results show that it is possible to obtain similar acceleration mechanisms by using lower density and thicker targets such as micron-scale Hydrogen jets, which are compatible with high-repetition rates. These findings open the possibility to achieve significantly higher proton energies in the future by appropriately matching the laser and target parameters.

Acknowledgement

This work was supported by the U.S. Department of Energy SLAC Contract No. DE-AC02-76SF00515. This work was also supported by the DOE LDRD program and the DOE Office of Science, Fusion Energy Science (FWP 100182). Simulations were conducted at the National Energy Research Scientific Computing Center (NERSC).

References

[1] M. Borghesi, D. H. Campbell, A. Schiavi, M. G. Haines, O. Willi, A. J. MacKinnon, P. Patel, L. A. Gizzi, M. Galimberti, R. J. Clarke, F. Pegoraro, H. Ruhl, and S. Bulanov, Phys. Plasmas **9**, 2214 (2002).

[2] S. V. Bulanova, T. Z. Esirkepov, V. S. Khoroshkov, A. V. Kuznetsov, and F. Pegoraro, Phys. Lett. A **299**, 240 (2002).

[3] M. Roth, T. E. Cowan, M. H.Key, S. P. Hatchett, C. Brown, W. Fountain, J. Johnson, D. M. Pennington, R. A. Snavely, S. C. Wilks, K. Yasuike, H. Ruhl, F. Pegoraro, S. V. Bulanov, E. M. Campbell, M. D. Perry, and H. Powell, Phys. Rev. Lett. **86**, 436 (2001).

[4] V. Malka, J. Faure, Y. A. Gauduel, E. Lefebvre, A. Rousse, and K. T. Phuoc, Nature Phys. **4**, 447 (2008);

[5] L. Robson, P. T. Simpson, R. J. Clarke, K. W. D. Ledingham, F. Lindau, O. Lundh, T. McCanny, P. Mora, D. Neely, C. G. Wahlstrom, M. Zepf, and P. McKenna, ibid. **3**, 58 (2007), and references therein.

[6] A. R. Smith, Med. Phys. 36, 556 (2009); V. Malka, S. Fritzler, G. Grillon, J. Chambaret, A. Antonetti, D. Hulin, E. Lefebvre, E. dHumieres, R. Ferrand, C. Albaret, and S. Meyroneinc, ibid. **31**, 1587 (2004).

[7] S. C. Wilks, A. B. Langdon, T. E. Cowan, M. Roth, M. Singh, S. Hatchett, M. H. Key, D. Pennington, A. MacKinnon, and R. A. Snavely Phys. of Plasmas **8**, 542 (2001).

[8] T. Esirkepov, M. Borghesi, S. V. Bulanov, G. Mourou, and T. Tajima, Phys. Rev. Lett. **92**, 175003 (2004).

[9] S. A. Gaillard, T. Kluge, K. A. Flippo, M. Bussmann, B. Gall, T. Lockard, M. Geissel, D. T. Offermann, M. Schollmeier, Y. Sentoku, and T. E. Cowan, Phys. Plasmas **18**, 056710 (2011).

[10] D. Haberberger, S. Tochitsky, F. Fiuza, et al., Nature Phys. **8**, 95 (2012).

[11] F. Fiuza, A. Stockem, E. Boella, et al., Phys. Rev. Lett. **109**, 215001 (2012).

[12] A. Macchi, A. S. Nindrayong, F. Pegoraro, Phys. Rev. E **85**, 046402 (2012).

[13] F. Fiuza, A. Stockem1, E. Boella, R. A. Fonseca, L. O. Silva, D. Haberberger, S. Tochitsky, W. B. Mori and C. Joshi, Phys. Plasmas **20**, 056304 (2013).

[14] S. S. Bulanov, V. Yu. Bychenkov, V. Chvykov, G. Kalinchenko, D. W. Litzenberg, T. Matsuoka, A. G. R. Thomas, L. Willingale, V. Yanovsky, K. Krushelnick, and A. Maksimchuck, Phys. Plasmas **17**, 1 (2010).

[15] Tatsufumi Nakamura, Sergei V. Bulanov, Timur Zh. Esirkepov, and Masaki Kando, Phys. Rev. Lett. **105**, 135002 (2010).

[16] M. H. Helle, D. F. Gordon, D. Kaganovich, Y.-H. Chen, and A. Ting, Proc. SPIE **9514**, 951409 (2015).

[17] S. Palaniyappan, B. M. Hegelich, H.-C. Wu, D. Jung, D. C. Gautier, L. Yin, B. J. Albright, R. P. Johnson, T. Shimada, S. Letzring, D. T. Offermann, J. Ren, C. Huang, R. Horlein, B. Dromey, J. C. Fernandez, and R. C. Shah, Nature Physics 8, 763 (2012); D. Jung, B. J. Albright, L. Yin, D. C. Gautier, R. Shah, S. Palaniyappan, S. Letzring, B. Dromey, H.-C. Wu, T. Shimada, R. P. Johnson, M. Roth, J. C. Fernandez, D. Habs, and B. M. Hegelich, New J. Phys. **15**, 123035 (2013).

[18] L. Yin, B. J. Albright, B. M. Hegelich, K. J. Bowers, K. A. Flippo, T. J. T. Kwan, and J. C. Fernandez, Phys. Plasmas, **14**, 056706 (2007).

[19] B. M. Hegelich, I. Pomerantz, L. Yin, H. C. Wu, D. Jung, B. J. Albright, D. C. Gautier, S. Letzring, S. Palaniyappan, R. Shah, K. Allinger, R. Horlein, J. Schreiber, D. Habs, J. Blakeney, G. Dyer, L. Fuller, E. Gaul, E. Mccary, A. R. Meadows, C. Wang, T. Ditmire, and J. C. Fernandez, New J. Phys. 15, 085015 (2013).

[20] A. Henig, D. Kiefer, K. Markey, D. C. Gautier, K. A. Flippo, S. Letzring, R. P. Johnson, T. Shimada, L. Yin, B. J. Albright, K. J. Bowers, J. C. Fernandez, S. G. Rykovanov, H.-C. Wu, M. Zepf, D. Jung, V. Kh. Liechtenstein, J. Schreiber, D. Habs, and B. M. Hegelich, PRL **103**, 045002 (2009).

[21] Y. Sentoku and A. J. Kemp, J. Comput. Phys., **227**, 6846 (2008).

[22] R. Mishra, P. Leblanc, Y. Sentoku, M. S. Wei and F. N. Beg, Phys. Plasmas **20**, 072704 (2013).

[23] P. Mora Phys. Rev. Lett., **90**, 185002 (2003).

[24] M. Passoni, and M. Lontano, Laser Part. Beams **22**, 163 (2004).

[25] J. Schreiber, F. Bell, F. Grner, U. Schramm, M. Geissler, M. Schnrer, S. Ter-Avetisyan, B. M. Hegelich, J. Cobble, E. Brambrink, J. Fuchs, P. Audebert, and D. Habs, Phys. Rev. Lett. **97**, 045005 (2006).

[26] W. L. Kruer and K. Estabrook, Phys. Fluids 0031-9171 **28**, 430 (1985).

[27] J. May, J. Tonge, F. Fiuza, R. A. Fonseca, L. O. Silva, C. Ren, and W. B. Mori, Phys. Rev. E **84**, 025401 (2011).

[28] A. I. Akhiezer, R. V. Polovin, "Theory of wave motion of an electron plasma" Sov. Phys., JETP **3**, 696-705 (1956).

[29] P. K. Kaw and J. M. Dawson, Phys. Fluids **13**, 472-481 (1970).

[30] A.V. Brantov, E. A. Govras, V. Yu. Bychenkov, and W. Rozmus, Phys. Rev. ST Accel. Beams **18**, 021301 (2015).

[31] E. d'Humires, A. Brantov, V. Yu. Bychenkov, and V. T. Tikhonchuk, Phys. Plasmas **20**, 023103 (2013).

[32] G. Mourou, T. Tajima, and S. V. Bulanov, Rev. Mod. Phys 78, 309 (2006); H. Daido, M. Nishiuchi, and A. S. Pirozhkov, Rep. Prog. Phys. 75, 056401 (2012); A. Macchi, M. Borghesi, and M. Passoni, Rev. Mod. Phys. 85, 751 (2013).

[33] A. Henig, D. Kiefer, K. Markey, D. C. Gautier, K. A. Flippo, S. Letzring, R. P. Johnson, T. Shimada, L. Yin, B. J. Albright, K. J. Bowers, J. C. Fernndez, S. G. Rykovanov, H.-C. Wu, M. Zepf, D. Jung, V. Kh. Liechtenstein, J. Schreiber, D. Habs, and B. M. Hegelich, Phys. Rev. Lett. **103**, 045002 (2009).

[34] T. Esirkopov, M. Yamagiwa and T. Tajima, Phys. Rev. Lett. **96**, 105001 (2006).

[35] L. Yin, B. J. Albright, B. M. Hegelich, and J. C. Fernandez. Laser and Particle Beams 24.2 (Jun 2006): 291-298